Differential modes of termination of amygdalothalamic and amygdalocortical projections in the monkey

Journal:	*The Journal of Comparative Neurology*
Manuscript ID:	JCN-06-0510.R2
Wiley - Manuscript type:	Research Article
Keywords:	driver, emotion, single axon, social behavior, synaptic bouton, zinc

Differential modes of termination of amygdalothalamic and amygdalocortical projections in the monkey

Toshio Miyashita[1]*, Noritaka Ichinohe[1, 2], and Kathleen S. Rockland[1, 3]

[1] Lab. for Cortical Organization and Systematics, Brain Science Institute, RIKEN
2-1 Hirosawa, Wako-shi, Saitama, 351-0198, Japan

[2] Graduate School of Medicine, Kyoto University,
Konoe-cho, Yoshida, Sakyo-ku, Kyoto, 606-8501, Japan

[3] Graduate School of Science and Engineering, Saitama University,
Sakura-ku, Saitama-shi, Saitama, 338-8570, Japan

Running title: Amygdalothalamic and -cortical terminations

Associate Editor: Dr. Joseph L. Price

Key words: driver, emotion, single axon, social behavior, synaptic boutons, zinc

*Correspondence to:
Toshio Miyashita, Ph.D.
Laboratory for Cortical Organization and Systematics
Brain Science Institute, RIKEN
2-1 Hirosawa, Wako-shi, Saitama, 351-0198, Japan
TEL: +81-48-462-1111
FAX: +81-48-467-6420
E-mail: toshio@brain.riken.jp

Supporting Grants:
We gratefully acknowledge research funding from Brain Science Institute, RIKEN and Grant-in-Aid for Scientific Research on Priority Areas “System study on higher-order brain functions” from the Ministry of Education, Culture, Sports, Science and Technology of Japan (Grant number: 18020032).

Abstract

The amygdala complex participates in multiple systems having to do with affective processes. It has been implicated in human disorders of social and emotional behavior, such as autism. Of the interconnected functional networks, considerable research in rodents and primates has focused on connections between the amygdala and orbitofrontal cortex (OFC). The amygdala projects to OFC by both a direct amygdalocortical (AC) pathway, and an indirect pathway through mediodorsal thalamus. In the rat, retrograde tracer experiments indicate that the AC and amygdalothalamic (AT) pathways originate from separate populations, and may therefore convey distinctive information, although the characteristics of these pathways remain unclear. To investigate this issue in monkeys, we made anterograde tracer injections in the basolateral amygdala complex (BLC; n=3). Three distinctive features were found preferentially associated with the AT or AC pathways. First, AT terminations are large (average diameter = 3.5 μm; range = 1.2-7.0 μm), and cluster around proximal dendrites, in contrast with small-bouton AC terminations. Second, AT terminations form small arbors (d ~ 0.1 mm), while AC are widely divergent (often > 1.0 mm long). The AT terminations features are reminiscent of large bouton, "driver" corticothalamic terminations. Finally, AC but not AT terminations are positive for zinc (Zn), a neuromodulator associated with synaptic plasticity. From these results, we suggest that AC and AT terminations originate from distinct populations in monkey as well as in rodent. Further work is necessary to determine the degree and manner of their segregation, and how these subsystems interact within a broader connectivity network.

Introduction

The amygdala complex participates in multiple distributed systems having to do with cognitive processes, such as emotion, reward representation, and stimulus-reward learning (Holland and Gallagher, 1999; LeDoux, 2000; Baxter and Murray, 2002; Everitt et al., 2003; Maren and Quirk, 2004). It has been implicated in human disorders of social and emotional behavior, such as autism (Amaral et al., 2003; Bachevalier and Loveland, 2006). Of the interconnected functional networks, considerable research has focused on the connections between the basolateral amygdala (BLA) and orbitofrontal cortex (OFC). In rats, electrophysiological recordings after lesions of either the BLA or OFC provide evidence of strong cooperative interactions, related to the encoding of information about expected outcomes and acquired value (Schoenbaum et al., 2003; Saddoris et al., 2005). In monkeys, combined unilateral lesions of the amygdala and OFC significantly disrupt affective processing (Izquierdo and Murray, 2004).

The broader amygdala-OFC circuit includes many interconnected structures. In humans and monkeys, these include the anterior cingulate cortex, ventral temporal cortex, and the superior temporal gyrus, as well as thalamic nuclei and the hippocampal formation (Cavada et al., 2000; Bachevalier and Loveland, 2006). Fuller understanding of subtle amygdala-related functions and their underlying substrates will require more information not only on the identity of pathway structures, but, importantly, on how they interact (Zald, 2003; Bennett and Hacker, 2005). As an example, work in humans has specifically implicated the medial temporal lobe in explicit memories about emotions, and the amygdala in implicit emotional memories (Bechara et al., 1995, LaBar et al., 1995); but the long-lasting vivid character of

explicit memories with emotional content has been attributed to amplifying effects on the cortex via the amygdala (Ledoux, 2000)

In monkeys, bilaterally symmetrical lesions of the amygdala, OFC, or mediodorsal (MD) thalamus all produce similar, severe postoperative learning impairments (Gaffan and Murray, 1990). These structures have all been related to reward-related functions (Baxter and Murray, 2002); but their specific functional contributions are not well-established. Moreover, little is known about the potential properties and interactions of what seem to be several parallel amygdalocortical (AC) pathways ("triadic architecture," Porrino et al., 1981); namely, a direct AC and indirect amygdalothalmo-cortical connection (through MD). As one step toward better understanding of these pathway dynamics, we have investigated morphological properties of the AC and AT pathways.

Anatomical evidence suggests that the two pathways originate from distinct neural populations, and therefore may be supposed to convey distinctive information. That is, in rats, injection of two retrograde tracers in the OFC and MD do not result in double-labeled neurons, even though the two populations are spatially intermixed (McDonald, 1987). Since there has tended to be greater collateralization in rodents than in primate (Mitchell and Macklis, 2005), we might expect similarly segregated subpopulations in monkey. Given the high degree of species specialization, however, direct substantiation of this point is desirable. Since the placement of double tracers is difficult, we chose to use anterograde tracer injections in the lateral and accessory basal nuclei in monkeys. By this means, we were able to demonstrate three distinctive features associated with each pathway. First, AT terminations form small arbors (~

0.1 mm in diameter), while AC terminations are widely divergent (> 1.0 mm in length). Second, AT terminations cluster around proximal dendrites and are conspicuously large, in contrast with small AC terminations. Third, AC but not AT terminations are positive for Zn, a neuromodulator associated with synaptic plasticity. Together, these results are consistent with an origin from separate neuron populations.

The AT terminations strongly resemble the large-bouton, small-arbor type2 cortico-thalamic (CT) connections ("driver"). This result raises the possibility of an especially effective AT system, with distinct temporal properties or processing modes. Finally, since the organization of thalamic circuitry is another level in the proposed amygdalo-thalamic-cortical circuit, we include data on bouton shape of some CT, as well as AT, terminations in MD.

Materials and Methods

Surgery and tracer injection

Three adult macaque monkeys (one *Macaca mulatta* and two *Macaca fuscata*) were used to demonstrate AT projections. All experimental protocols were reviewed and approved by the Experimental Animal Committee of the RIKEN Institute, and were carried out in accordance with the National Institutes of Health Guide for the Care and Use of Laboratory Animals (NIH Publications No. 80-23), revised 1996. We attest that every effort was made to minimize the number of animals used and their suffering.

In preparation for surgery, the monkeys were tranquilized by an i.m. injection of ketamine (11 mg/kg), and subsequently deeply anesthetized with barbiturate

anesthesia (35 mg/kg Nembutal, i.p.). Surgery was carried out under sterile conditions; and heart rate, EEG, and body temperature were monitored throughout the procedure. First, a bilateral craniotomy was opened dorsally, overlying the approximate position of the amygdala complex, as determined by stereotaxic coordinates (Paxinos et al., 2000). Ultrasound imaging was carried out (LOGIQ9, GE Medical Systems, Milwaukee, WI; Tokuno et al., 2002; Imura and Rockland, 2006) in order to visualize the target amygdala, and the location and depth of an injection needle coated with Teflon (New TEF coat, Finechemical Japan, Tokyo Japan). Maximum resolution in ultrasound was achieved by imaging the contralateral side. A single injection of 1-3 µl of the anterograde tracer biotinylated dextran amine (BDA; Molecular Probes, Eugene, OR; 3,000 and 10,000 MW in a 1:1 proportion, diluted to 10% in 12.5 mM phosphate buffered saline, PBS) was made by pressure through a 10 µl Hamilton syringe). Injections were located in the accessory basal nucleus (n=1) or lateral nucleus (n=2; see Fig. 1).

In addition, two brains were re-analyzed from a previous study based on injections of anterograde tracers in parietal association cortices (Fig. 2; see also Fig. 1 of Zhong and Rockland, 2003**).** Three other brains were available with anterograde tracer injections in prefrontal areas 45 or 12 (Fig. 2; and Ichinohe and Rockland, 2001).

Animals were allowed to recover and survived 17-21 days after the injection. As a terminal procedure, they were then re-anesthetized with ketamine (11 mg/kg, i.m.) and Nembutal (overdose, 75 mg/kg i.p.) and perfused transcardially. For one animal (case 300), the perfusate solutions were, in sequence: saline containing 0.5% sodium nitrite, 4 liters of 4% paraformaldehyde (PFA) in 0.1 M phosphate buffer (PB; pH 7.4)

for 30 min, and chilled 0.1 M phosphate buffer (PB) with 10%, 20%, and 30% sucrose.

For Zn histochemistry, the two other monkeys (case 298 and R100) received intravenous injection of saline with 10% sodium sulfide (200 mg/kg). Two minutes after the injection, the animals were perfused transcardially, in sequence, with saline containing 0.5% sodium nitrite with 4% PFA in 0.1 M PB for 30 min, and with chilled 0.1 M PB with 10% and 20% sucrose. Brains were removed from the skull; and small cortical blocks were trimmed out through area 25 of prefrontal cortex for EM processing. The larger blocks were immersed into 30% sucrose in 0.1 M PB for continued processing for light microscopy.

Histology for light microscopy

After the brain sank, blocks were trimmed and sectioned serially in the coronal plane by using a freezing microtome (at 50 μm thickness). Freefloating sections were processed for BDA histochemistry. To visualize subdivisions within the amygdala, some sections through the injection site and its vicinity were selected for parvalbumin (PV) immunohistochemistry.

For BDA histochemistry, sections were incubated for 20-24 hrs in avidin-biotin complex (one drop of reagents per 7 ml 0.1 M PB, ABC Elite kits; Vector, Burlingame, CA) at room temperature. In the final step, BDA was demonstrated by 3,3'-diaminobenzidine tetrahydrochloride (DAB) histochemistry with the addition of 0.03% nickel-ammonium sulfate. For the brains with parietal or prefrontal cortical injections, strict serial sections were prepared for BDA histochemistry.

For PV immunohistochemistry, sections were incubated for 1 hr in 0.1 M phosphate-buffered saline (PBS; pH 7.4) containing 0.5% Triton X-100 and 5% normal goat serum (PBS-TG) at room temperature, and then 40-48 hrs at 4 ˚C with PBS-TG containing mouse monoclonal anti-PV antibody (Swant, Bellinzona, Switzerland; 1:50,000). After rinsing, the sections were placed in PBS-TG containing biotinylated goat anti-mouse IgG (Vector, Burlingame, CA; 1:200) for 1.5 hrs at room temperature. Immunoreactivity was visualized by avidin biotin complex incubation (ABC Elite kits; Vector, Burlingame, CA) followed by DAB histochemistry with 0.03% nickel ammonium sulfate.

Four brains were available from a previous study, which had been reacted for Zn histochemistry (Ichinohe and Rockland, 2005a). These were examined for area and laminar distribution of Zn-positive (Zn+) terminations. Briefly, the IntenSE M silver Enhancement kit (Amersham International, Little Chalfont, Bucks, UK) was used to intensify Zn signals (Danscher et al., 1987; De Biasi and Bendotti, 1988; Ichinohe and Rockland, 2005a). Sections were washed thoroughly with 0.1 M PB, followed by 0.01 M PB. A one-to-one cocktail of the IntenSE M kit solution and 33% gum arabic solution was used as a reagent. Development of reaction products was monitored under a microscope and terminated by rinsing the sections in 0.01 M PB and, subsequently, several times in 0.1 M PB.

Further antibody description

The mouse monoclonal anti-PV antibody used here (Swant: Bellinzona, Switzerland; Code No: 235, Lot No: 10-11 [F]) was prepared against purified carp-muscle PV (Celio et al., 1988). It specifically stains the ^{45}Ca-binding spot of PV (MW 12,000 and IEF 4.9) in a two-dimensional immunoblot (manufacture's technical information). Staining pattern and density of PV in the amygdala and MD bythis antibody were consisted with previous descriptions in monkey (Jones and Hendry, 1989; Pitkänen and Amaral, 1993).

EM analysis of boutons containing Zn and BDA

Vibratome-cut coronal sections (50 μm thick) were prepared. These were washed thoroughly with 0.1 M PB, followed by distilled water. The silver enhancement kit was used to intensify Zn signals as described above. Staining intensity during development was carefully monitored by periodic visual inspection under a low power microscope. Development was terminated by rinsing the sections in distilled water and, subsequently, several times in 0.1 M PB. Several sections were selected and further processed for peroxidase-histochemistry for BDA. The procedures for BDA visualization were basically as described above for light microscopy, except that Triton X-100 was omitted in all solutions, and nickel was omitted for the DAB step. To improve antibody penetration in the absence of Triton X-100, after silver enhancement, sections were incubated in 20% sucrose for 2 hrs, and then were freeze-thawed with liquid nitrogen.

Sections stained either for Zn alone, or for Zn and BDA were osmicated, dehydrated, and flat-embedded in resin (Araldite M; TAAB, Aldermaston, UK). From the plastic

sections, we further trimmed out upper layers (from the layer 1/2 border to upper layer 3) and lower layers (layers 5 and 6). Ultrathin sections were collected on formvar-coated, single-slot grids, and examined with an electron microscope (JEM 2000-EX; JEOL, Tokyo, Japan). For quantification, electron micrographs were taken at a magnification of 30,000 from randomly selected fields that included BDA-labeled elements in the neuropil. Data were collected from one tissue sample from two animals, and digital pictures were recorded. On each micrograph, profiles postsynaptic to Zn+ terminals were identified and classified as spines or dendrites based on standard ultrastructural criteria (Peters et al., 1991). That is, profiles were identified as spines based on size (0.3-1.5 μm in diameter), presence of spine apparatus, and/or absence of mitochondria or microtubules. Dendrites were identified by their larger size (0.5 μm or greater in diameter), and presence of microtubules and mitochondria.

When critical steps are controlled (i.e. low sulphide concentrations and fixed amplification parameters), as in Danscher's procedure (Danscher et al., 1987, 1996), the sulfide method is reported to reveal Zn specifically associated to synaptic vesicles. (See Methods, Ichinohe and Rockland, (2005a) for further discussion that the signal is Zn, as opposed to other metal ions.)

Analysis

In the LM, tissue was scanned at lower magnification (100x or 200x) for distribution of label, and at higher magnification (400x or 1,000x oil) for inspection of bouton features. BDA-labeled terminal fields in the thalamus were analyzed for axon configuration, convergence, and divergence by using a microscope equipped with

camera lucida to map serial sections over short sequences (5-20 sections or 0.25-1.0 mm). Focus analysis of BDA-labeled terminations in the thalamus was carried out by low magnification photography of 8 serial sections. These were merged manually with Photoshop software (transparent layer mode).

Light and fluorescent microscope photographs were taken on digital cameras (Axioscop2 and Axiocam, Carl Zeiss Vision, Munchen-Hallbergmoos, Germany). Size, brightness, and contrast of images were adjusted to coincide with the real image, by using Photoshop 7.0 software (Adobe Systems, San Jose, CA, USA).

Nomenclature

Amygdaloid complex. The amygdaloid nuclear subdivisions mainly follow the descriptions of Price et al (1987), as modified by Amaral and Bassett (1989) and Pitkänen and Amaral (1998). (See also, Ichinohe and Rockland, 2005a.) For the three brains with amygdala injections, subdivisions were determined mainly by reference to PV-immunoreactivity and the pattern of intrinsic connections. In this study, we grouped three nuclei (lateral, basal, and accessory basal nuclei) as a basolateral complex (BLC).

Mediodorsal thalamic nucleus. For the mediodorsal thalamic nuclear subdivisions, we used four standard subdivisions, mainly following Aggleton and Mishkin (1984) and Goldman-Rakic and Porrino (1985). In this study, we focused on the magnocellular portion of mediodorsal nucleus (MDmc). MDmc is located rostrally and medially. The parvicellular portion (MDpc) is located lateral to the MDmc.

Orbitofrontal cortex. For the orbitofrontal subdivisions, we followed the description of Amaral and Price (1984), Ray and Price (1993), and Cavada et al (2000).

Results

Location of injection sites

The location of the injection sites within the amygdala were identified by comparison with published maps, and with reference to interspersed sections stained with anti-PV antibody (Table 1 and Fig. 1). The most medial injection (case 298) was mainly in the parvicellular subdivision of the accessory basal nucleus (ABpc). Labeled terminations are evident in the periamygdaloid cortex and/or posterior cortical nucleus, as a result of intrinsic connectivity, and also at the border of the lateral nucleus and the parvicellular division of the basal nucleus (Bpc; arrowhead in Fig. 1C). Terminations in this lateral location may have resulted from uptake along the track of the injection needle. In the other two cases (case 300 and R100), the BDA injection was located in the lateral nucleus. In case 300, the injection was made by a vertical approach, parallel to the midline, and was centered in the dorsal intermediate division of the lateral nucleus. Intrinsic terminations are observed in AB (Fig. 1B). In case R100, the injection was centered in the ventral subdivision of the lateral nucleus. In this animal, an oblique approach was employed in order to control for possible spread of injected BDA in the vertical approach (case 300). With this more ventral and caudal injection site, intrinsic terminations were observed in ABpc (Fig. 1D and E).

Projection Focus

In all three cases, BDA-labeled terminations occurred in the MD, mainly in the anterior two-thirds of the magnocellular subdivision (MDmc). Despite the relatively large injections (d > 1.0mm), the projection focus was consistently patchy, as previously reported from studies using autoradiography in monkeys (Aggleton and Mishkin, 1984; Russchen et al., 1987). With the single axon resolution of BDA, it was

possible to distinguish that arbors occurred both singly and in clusters of 8-10 (Fig. 3). Serial section reconstruction (through 400 μm) confirmed that apparent patches were in fact distinct and did not merge into rods or other larger structures. For individual arbors, center-to-center spacing is about 0.15-0.45 mm. The larger terminal clusters were about 1 mm (dorso-ventral) x 0.4 mm (medio-lateral; Fig. 3I).

Single arbors

Arbors were generally small (longest diameter ≤ 80 μm), and tended to be slightly elongated in the dorso-ventral dimension. Very commonly, arbors had a peculiar, spokelike ("starfish") shape, with multiple tightly packed synapses aligned in a row (Fig. 4). What appeared to be aggregations of more spherical arbors were also evident.

The spoke-like arbors often occurred close to an unlabeled cell body, as if the spokes were targeting the proximal dendrites of a single neuron or adjoining neurons (Figs. 4 and 5). In a related set of experiments, a similar spokelike shape of CT terminations could be detected in the MD nucleus after large injections of BDA in the inferior parietal lobule. Moreover, the CT spokes could sometimes be observed in close association with a retrogradely filled thalamocortical projection neuron (Fig. 5B).

From partial reconstructions of three axon segments, we ascertained that single axons could have multiple arbors. In one axon (case 298), three arbors were detected. Two arbors converged in a single focus, after a proximal bifurcation, and a third arbor diverged to a locus 0.5 mm offset (Figs. 6 and 7). Another arbor, originating from a separate segment, intermingled with the two converging arbors. Branched axon segments occurred frequently, and this would suggest that axons commonly have

multiple arbors (Fig. 7). Many thick axons were apparent within the projection focus (Fig. 7).

Bouton Shape: AT and AC

As a population, the AT terminations are distinctly large, with an average diameter of 3.17, 3.67, or 3.63 μm in the three cases (Table 2 and Figs. 7 and 8). Boutons occur singly, in small clusters of 5-7, or in tightly arrayed rows. Very large boutons (longest diameter ~ 7.0 μm) can easily be detected, and these are often surrounded by threadlike processes (Fig. 8D, E). It is important to note that, even within a single arbor, the boutons show a range of sizes. The longest axis can range from < 1.5 μm to about 7.0 μm (Table 2). Small, stalked boutons occur singly or in combination with large boutons (Fig. 8B-E), and there are also longer, filopodia-like structures. The possibility that some small and large boutons may occur together has been recently noted for prefrontal projections to the thalamic reticular nucleus (Zikopoulos and Barbas, 2006; and see Fig. 21 in Rockland, 1998).

For comparison, we inspected brains with cortical injections in parietal (n=2) or frontal (n=3) areas. The parietal injections produced terminations with large boutons and small arbors (Figs. 5B, C and 9D), two characteristics of type 2 CT terminations (Ojima, 1994; Rockland, 1996; Sherman and Guillery, 1998, 2001; Rouiller and Welker, 2000). These were overall very similar to the configuration of AT terminations (compare Fig. 8B and D). The prefrontal injections resulted in terminations with small, mainly stalked boutons, which were arrayed along long segments of the main axon (Fig. 9C). These two characteristics together identify type 1 CT terminations. Some of the small boutons of type 1 terminations may be

indistinguishable from the smallest boutons within a type 2 arbor, but the density is different, and the arbor shape ("drumstick") provides a second, unambiguous diagnostic criterion.

In contrast with large bouton AT terminations, the AC terminations consist of a mix of small beaded and stalked boutons (Fig. 9A). These are aligned along long segments, which tend to travel parallel to the pia, especially in the upper layers (see also, Fig. 5 in Freese and Amaral, 2005). The small bouton AC terminations can easily be distinguished from the very specialized ("drumstick") type 1 CT terminations (Fig. 9A vs. 9C).

AC terminations are Zn+

Synaptic Zn is used by a subset of cortico-cortical terminations, and also by cortical projections from the hippocampal formation and from the amygdala (Frederickson and Danscher, 1990; Slomianka, 1992; Brown and Dyck, 2005; Ichinohe and Rockland, 2005b). Terminations to most thalamic nuclei are negative for Zn, and so is the thalamo-recipient layer 4 in cortex (Fig. 10). In cortex, histochemistry for Zn shows area-specific differences in density and laminar distribution which partially match with those of AC terminations. In the orbitofrontal cortex, synaptic Zn is dense in layers 1b, 2, upper 3, 5, and 6 (Figs. 10 and 11; and Carmichael and Price, 1994; Ichinohe and Rockland, 2004). These are the same layers that receive dense AC terminations (Fig. 10B; and Amaral and Price, 1984; Freese and Amaral, 2005, 2006).

In two of our three cases, brains were prepared with a perfusion of sodium sulfide to precipitate synaptic Zn, and tissue was double reacted for BDA and silver

intensification to visualize Zn+ terminals. After subsequent processing for EM, tissue was inspected and BDA-labeled AC terminations were evaluated as positive or negative for Zn (Fig. 12). In case 298, all of 222 BDA-labeled terminations were Zn+ (122 in the upper layers, and 100 in the lower layers). The result was similar for 209 BDA-labeled terminations in case R100 (109 in the upper layers and 100 in the lower layers). Some contacts were on dendritic shafts, but most contacts were with spines (90% in case 298; 91% in case R100). Synapses were small, with a mean smallest diameter of 0.65 μm (range = 0.3-0.9 μm). About 25% of the synapses could be scored as perforated (in case 298: 32 synapses or 26% in the supragranular layers, and 24 synapses or 24% in the infragranular layers; in case R100: 24 synapses or 22% in the supragranular layers, and 28 synapses or 28% in the infragranular layers).

Discussion

The amygdala is an important component in the circuitry for generating the emotional context of situations and events (Sugase-Miyamoto and Richmond, 2005; Paton et al., 2006). The amygdala is not the generator of specific emotional responses, but rather operates to somehow code and process facial movements, eye-gaze directions, body postures, and other signals basic to social and emotional responses (Amaral et al., 2003; Bachevalier and Loveland, 2006). In rodents, the anatomic network underlying fear conditioning has been partially elucidated and shown to involve the convergence of sensory stimuli about the conditioned and unconditioned stimulus in the lateral nucleus (LeDoux et al., 1990; Maren et al., 1996; review in Maren, 2001; Wilensky et al., 2006). The possible mechanisms of more abstract associative conditions are less understood (Zald, 2003; Liddell et al., 2005; Phelps and LeDoux, 2005).

The present investigation has focused on the interconnections of the amygdala, MDmc, and orbitofrontal cortex. Our data support the likelihood that in monkey, as in rat, the AC and AT projections originate from separate populations in the BLC. In rat, this conclusion is based on retrograde tracer injections (McDonald, 1987), where no double-labeled cells could be detected. Our results are more indirect, but together are consistent with two separate populations of projection neurons. That is, we report three morphological features that distinguish AC vs. AT terminations: bouton size (large for AT, small for AC), arbor size (small for AT, widespread for AC), and the presence (for AC) or absence (for AT) of synaptic Zn (Fig. 13). Both bouton size and the presence or absence of synaptic Zn are functionally relevant features, with implications for synaptic efficacy, as discussed below.

Amygdalo-thalamic terminations: Driving?

One of the most striking features of AT terminations from both the accessory basal and lateral nuclei is the large bouton size. This feature appears to be conserved across species, as several ultrastructural studies in MD of rats report that the AT terminations are large and excitatory ("large round," LR). Additionally, EM visualization demonstrates that AT terminations preferentially target proximal dendrites of some relay cells, usually as part of glomerular specializations (Kuroda and Price, 1991; and for LM, see Fig. 5 of Bouwmeester et al., 2002). Consistent with the second result, AT terminations in our material are frequently found in association with cell bodies; and it seems likely that EM studies would demonstrate a similar proximal dendritic localization.

The large bouton size recalls type 2 CT terminations, which are also characterized by large, proximally situated boutons and small arbors (Rockland, 1996; Rouiller and Welker, 2000; Taktakishvili et al., 2002). In the CT system, these properties have been regarded as denoting a "driving" influence, by analogy with primary sensory afferents (Sherman and Guillery, 1998, 2001); and a reasonable prediction from our results is that AT terminations might have a comparable synaptic dynamics.

Several other inputs to MDmc have been established as large bouton (rat piriform cortex: Kuroda et al., 1992; monkey parietal cortex: Taktakishvili et al., 2002 and Fig. 5B, C). Further work is important to determine how these inputs converge and interact; for example, do they target the same or separate post-synaptic populations? In particular, both AT and type 2 CT terminations are patchy, and each appears to contact only a small subpopulation within the MD. In addition, the size and configuration of AT terminations are variable. Although the average bouton diameter of AT terminations is 3-4 μm, this number includes both very large, giant boutons (long diameter > 7.0 μm) as well as conventionally small boutons (diameter ~ 1.2 μm); and within a single arbor, boutons can be single, in clusters, or in rows of tightly adjoining boutons. Synaptic efficacy will need to be defined at the level of individual synapses, even within a single arbor.

We note that CT terminations in MD from prefrontal areas are predominantly type 1, small bouton (Schwartz et al., 1991). This is based in part on retrograde tracer injections in MD, which demonstrate that CT projection neurons are mainly in layer 6 (Giguere and Goldman-Rakic, 1998). This is the home layer of neurons that are considered to give rise to type 1 terminations (Ojima, 1994; Kakei and Shinoda,

2001). In addition, in our material, anterograde tracer injections in area 45 and lateral area 12 (case R42) result in almost exclusively type 1 CT terminations (Fig. 9C). This may indicate that CT terminations have a more "modulatory" role, in relation to other cortical inputs and AT inputs.

Amygdalo-cortical terminations: Modulating?

In this report, we provide evidence that the AC and AT pathways originate from separate populations and have distinctive morphological features. Previous work has often compared the basal and lateral amygdala nuclei to cortical structures (Braak and Braak, 1983; Carlsen and Heimer, 1986, 1988; Swanson and Petrovich, 1998; Price, 2003); and in this framework, one might wonder whether the large bouton AT terminations are "like" CT terminations from layer 5, whereas the AC are more "like" cortical terminations. Morphologically, AC terminations are small and arranged along widely divergent arbors (see also, Freese and Amaral, 2005, 2006). At LM resolution, AC bouton morphology is similar to that of most cortico-cortical terminations (feedforward, feedback, or horizontal intrinsic), but is distinct from type 1 CT terminations, where the small boutons are overwhelmingly stalked ("drumstick," Rockland, 1996; Rouiller and Welker, 2000; Kultas-Ilinsky et al., 2003).

In frontal areas, AC terminations occur in two strata, mainly in layers 2, 3 and 5, 6. In the upper layers, at least, AC terminations may be supposed to terminate largely on distal apical dendrites. Thus, a key question for future investigation concerns the precise circuitry of the direct AC pathway vs. the two-stage AT-TC pathways, and whether these converge on the same neurons, even if on different dendritic domains.

AC synapses are frequently perforated (about 25%; present report and Freese and Amaral, 2006), and, as shown here, they all appear to contain Zn. Zn-positive projection neurons can also be demonstrated in the amygdala by cortical injections of sodium selenite (Ichinohe and Rockland, 2005b). Currently, synaptic Zn is thought to act in a neuromodulatory role, with significant influence on plasticity effects. It is released in an activity- and calcium-dependent fashion and interacts with many receptors, ion channels, and neurotrophic factors (see for review: Cuajungco and Lees, 1997; Frederickson et al., 2000, 2005; Sensi et al., 2004; Smart et al., 2004). Thus, the presence of synaptic Zn is a hint that these AC terminations may have a high degree of plasticity.

Consistent with a more plastic quality, AC terminations show continued sprouting into early adulthood in rats, peaking at P45 in layer 2 and continuing to increase through P120 in layer 5 (Cunningham et al., 2002). By contrast, AT terminations are reported to be stable from P7 (Bouwmeester et al, 2002).

Summary

The functional organization of parallel and re-entrant pathways is a central problem, and has been frequently discussed in the context of corticocortical (Tononi et al., 1992), corticothalamic (Crick and Koch, 1998; Sherman and Guillery, 2001), and corticohippocampal (Lavenex and Amaral, 2000; Kloosterman et al., 2003), as well as amygdalocortical connections (Zald, 2003; Williams et al., 2006). In one interesting result that regards *inputs* to the amygdala, recent imaging experiments have supported a dissociation of subcortical (collicular-pulvinar) and cortical inputs, such that these are implicated with different levels of awareness; that is, respectively, emotional responsivity without (subcortical) or with (cortical) awareness (Williams et al, 2006). These and other studies suggest fruitful grounds for investigating the connectivity networks , distinctive activation patterns, and resulting behaviors.

Our results have demonstrated several differences in the AC and AT pathways (Fig. 13). Together, these differences strongly suggest that, as in rats, the AC and AT pathways originate from separate populations, although there are obviously multiple opportunities for convergence and interaction. For example, the amygdala and OFC both project to the claustrum (Majak et al., 2002) and to the nucleus accumbens (Russchen et al., 1985; Friedman et al., 2002; Price, 2003); and these broader connectivity loops may be supposed to play a fundamental role in amygdala associative functions.

Acknowledgment

We thank Yoshiko Abe and Hiromi Mashiko for their excellent technical assistance; Hiroko Katsuno for her elegant electron microscopic work; and all members of the Laboratory for Cortical Organization and Systematics at the Brain Science Institute, RIKEN for their helpful colleagueality, discussion and comments. Dr. Ray Guillery kindly commented on a pre-final draft of the manuscript.

Abbreviations

ABmc	accessory basal nucleus, magnocellular nucleus
ABpc	accessory basal nucleus, parvicellular nucleus
acb	accumbens nucleus
amts	anterior middle temporal sulcus
ars	arcuate sulcus
Bmc	basal nucleus, magnocellular division
Bpc	basal nucleus, parvicellular division
cd	caudate nucleus
CE	central nucleus
cgs	cingulate sulcus
cs	central sulcus
HF	hippocampus formation
iar	inferior arcuate sulcus
ios	inferior occipital sulcus
ips	intraparietal sulcus
las	lateral sulcus
Ld	lateral nucleus, dorsal division
Ldi	lateral nucleus, dorsal intermediate division
lf	lateral fissure
lg	latetal geniculate nucleus
lus	lunate sulcus
Lv	laeral nucleus, ventral division
md	mediodorsal thalamic nucleus
ME	medial nucleus

opt	optic tract
PAC3	periamygdaloid cortex 3
PL	paralaminar nucleus
pmts	posterior middle temporal sulcus
ps	principal sulcus
pu	putamen
rf	rhinal fissure
sar	superior arcuate sulcus
sts	superior temporal sulcus
vl	ventrolateral thalamic nucleus
wm	white matter

Literature cited

Aggleton JP, Mishkin M. 1984. Projections of the amygdala to the thalamus in the cynomolgus monkey. J Comp Neurol 222(1):56-68.

Amaral DG, Bassett JL. 1989. Cholinergic innervation of the monkey amygdala: an immunohistochemical analysis with antisera to choline acetyltransferase. J Comp Neurol 281(3):337-361.

Amaral DG, Bauman MD, Capitanio JP, Lavenex P, Mason WA, Mauldin-Jourdain ML, Mendoza SP. 2003. The amygdala: is it an essential component of the neural network for social cognition? Neuropsychologia 41(4):517-522.

Amaral DG, Price JL. 1984. Amygdalo-cortical projections in the monkey (Macaca fascicularis). J Comp Neurol 230(4):465-496.

Bachevalier J, Loveland KA. 2006. The orbitofrontal-amygdala circuit and self-regulation of social-emotional behavior in autism. Neurosci Biobehav Rev 30(1):97-117.

Baxter MG, Murray EA. 2002. The amygdala and reward. Nat Rev Neurosci 3(7):563-573.

Bechara A, Tranel D, Damasio H, Adolphs R, Rockland C, Damasio AR. 1995. Double dissociation of conditioning and declarative knowledge relative to the amygdala and hippocampus in humans. Science 269(5227):1115-1118.

Bennett MR, Hacker PM. 2005. Emotion and cortical-subcortical function: conceptual developments. Prog Neurobiol 75(1):29-52.

Bouwmeester H, Wolterink G, van Ree JM. 2002. Neonatal development of projections from the basolateral amygdala to prefrontal, striatal, and thalamic structures in the rat. J Comp Neurol 442(3):239-249.

Braak H, Braak E. 1983. Neuronal types in the basolateral amygdaloid nuclei of man. Brain Res Bull 11(3):349-365.

Brown CE, Dyck RH. 2005. Retrograde tracing of the subset of afferent connections in mouse barrel cortex provided by zincergic neurons. J Comp Neurol 486(1):48-60.

Carlsen J, Heimer L. 1986. A correlated light and electron microscopic immunocytochemical study of cholinergic terminals and neurons in the rat amygdaloid body with special emphasis on the basolateral amygdaloid nucleus. J Comp Neurol 244(1):121-136.

Carlsen J, Heimer L. 1988. The basolateral amygdaloid complex as a cortical-like structure. Brain Res 441(1-2):377-380.

Carmichael ST, Price JL. 1994. Architectonic subdivision of the orbital and medial prefrontal cortex in the macaque monkey. J Comp Neurol 346(3):366-402.

Cavada C, Company T, Tejedor J, Cruz-Rizzolo RJ, Reinoso-Suarez F. 2000. The anatomical connections of the macaque monkey orbitofrontal cortex. A review. Cereb Cortex 10(3):220-242.

Celio MR, Baier W, Scharer L, de Viragh PA, Gerday C. 1988. Monoclonal antibodies directed against the calcium binding protein parvalbumin. Cell Calcium 9(2):81-86.

Crick F, Koch C. 1998. Constraints on cortical and thalamic projections: the no-strong-loops hypothesis. Nature 391(6664):245-250.

Cuajungco MP, Lees GJ. 1997. Zinc metabolism in the brain: relevance to human neurodegenerative disorders. Neurobiol Dis 4(3-4):137-169.

Cunningham MG, Bhattacharyya S, Benes FM. 2002. Amygdalo-cortical sprouting continues into early adulthood: implications for the development of normal and abnormal function during adolescence. J Comp Neurol 453(2):116-130.

Danscher G. 1996. The autometallographic zinc-sulphide method. A new approach involving in vivo creation of nanometer-sized zinc sulphide crystal lattices in zinc-enriched synaptic and secretory vesicles. Histochem J 28(5):361-373.

Danscher G, Norgaard JO, Baatrup E. 1987. Autometallography: tissue metals demonstrated by a silver enhancement kit. Histochemistry 86(5):465-469.

De Biasi S, Bendotti C. 1998. A simplified procedure for the physical development of the sulphide silver method to reveal synaptic zinc in combination with immunocytochemistry at light and electron microscopy. J Neurosci Methods 79(1):87-96.

Everitt BJ, Cardinal RN, Parkinson JA, Robbins TW. 2003. Appetitive behavior: impact of amygdala-dependent mechanisms of emotional learning. Ann N Y Acad Sci 985:233-250.

Frederickson CJ, Danscher G. 1990. Zinc-containing neurons in hippocampus and related CNS structures. Prog Brain Res 83:71-84.

Frederickson CJ, Koh JY, Bush AI. 2005. The neurobiology of zinc in health and disease. Nat Rev Neurosci 6(6):449-462.

Frederickson M, Neitzel JJ, Miller EH, Reuter S, Graner T, Heller J. 2000. The implementation of bedside bladder ultrasound technology: effects on patient and cost postoperative outcomes in tertiary care. Orthop Nurs 19(3):79-87.

Freese JL, Amaral DG. 2005. The organization of projections from the amygdala to visual cortical areas TE and V1 in the macaque monkey. J Comp Neurol 486(4):295-317.

Freese JL, Amaral DG. 2006. Synaptic organization of projections from the amygdala to visual cortical areas TE and V1 in the macaque monkey. J Comp Neurol 496(5):655-667.

Friedman DP, Aggleton JP, Saunders RC. 2002. Comparison of hippocampal, amygdala, and perirhinal projections to the nucleus accumbens: combined anterograde and retrograde tracing study in the Macaque brain. J Comp Neurol 450(4):345-365.

Gaffan D, Murray EA. 1990. Amygdalar interaction with the mediodorsal nucleus of the thalamus and the ventromedial prefrontal cortex in stimulus-reward associative learning in the monkey. J Neurosci 10(11):3479-3493.

Giguere M, Goldman-Rakic PS. 1988. Mediodorsal nucleus: areal, laminar, and tangential distribution of afferents and efferents in the frontal lobe of rhesus monkeys. J Comp Neurol 277(2):195-213.

Goldman-Rakic PS, Porrino LJ. 1985. The primate mediodorsal (MD) nucleus and its projection to the frontal lobe. J Comp Neurol 242(4):535-560.

Holland PC, Gallagher M. 1999. Amygdala circuitry in attentional and representational processes. Trends Cogn Sci 3(2):65-73.

Ichinohe N, Rockland KS. 2001. Prefrontal cortical projections to visual-related areas in macaque monkey. Neurosci Res Supplement 25(The 24th Annual meeting of the JAPAN Neuroscience society, Abstracts):PA3-061.

Ichinohe N, Rockland KS. 2004. Region specific micromodularity in the uppermost layers in primate cerebral cortex. Cereb Cortex 14(11):1173-1184.

Ichinohe N, Rockland KS. 2005a. Distribution of synaptic zinc in the macaque monkey amygdala. J Comp Neurol 489(2):135-147.

Ichinohe N, Rockland KS. 2005b. Zinc-enriched amygdalo- and hippocampo-cortical connections to the inferotemporal cortices in macaque monkey. Neurosci Res 53(1):57-68.

Imura K, Rockland KS. 2006. Long-range interneurons within the medial pulvinar nucleus of macaque monkeys. J Comp Neurol 498(5):649-666.

Izquierdo A, Murray EA. 2004. Combined unilateral lesions of the amygdala and orbital prefrontal cortex impair affective processing in rhesus monkeys. J Neurophysiol 91(5):2023-2039.

Jones EG, Hendry SH. 1989. Differential Calcium Binding Protein Immunoreactivity Distinguishes Classes of Relay Neurons in Monkey Thalamic Nuclei. Eur J Neurosci 1(3):222-246.

Kakei S, Na J, Shinoda Y. 2001. Thalamic terminal morphology and distribution of single corticothalamic axons originating from layers 5 and 6 of the cat motor cortex. J Comp Neurol 437(2):170-185.

Kloosterman F, Van Haeften T, Witter MP, Lopes Da Silva FH. 2003. Electrophysiological characterization of interlaminar entorhinal connections: an essential link for re-entrance in the hippocampal-entorhinal system. Eur J Neurosci 18(11):3037-3052.

Kultas-Ilinsky K, Sivan-Loukianova E, Ilinsky IA. 2003. Reevaluation of the primary motor cortex connections with the thalamus in primates. J Comp Neurol 457(2):133-158.

Kuroda M, Murakami K, Kishi K, Price JL. 1992. Distribution of the piriform cortical terminals to cells in the central segment of the mediodorsal thalamic nucleus of the rat. Brain Res 595(1):159-163.

Kuroda M, Price JL. 1991. Synaptic organization of projections from basal forebrain structures to the mediodorsal thalamic nucleus of the rat. J Comp Neurol 303(4):513-533.

LaBar KS, LeDoux JE, Spencer DD, Phelps EA. 1995. Impaired fear conditioning following unilateral temporal lobectomy in humans. J Neurosci 15(10):6846-6855.

Lavenex P, Amaral DG. 2000. Hippocampal-neocortical interaction: a hierarchy of associativity. Hippocampus 10(4):420-430.

LeDoux JE. 2000. Emotion circuits in the brain. Annu Rev Neurosci 23:155-184.

LeDoux JE, Cicchetti P, Xagoraris A, Romanski LM. 1990. The lateral amygdaloid nucleus: sensory interface of the amygdala in fear conditioning. J Neurosci 10(4):1062-1069.

Liddell BJ, Brown KJ, Kemp AH, Barton MJ, Das P, Peduto A, Gordon E, Williams LM. 2005. A direct brainstem-amygdala-cortical 'alarm' system for subliminal signals of fear. Neuroimage 24(1):235-243.

Majak K, Pikkarainen M, Kemppainen S, Jolkkonen E, Pitkänen A. 2002. Projections from the amygdaloid complex to the claustrum and the endopiriform nucleus: a Phaseolus vulgaris leucoagglutinin study in the rat. J Comp Neurol 451(3):236-249.

Maren S. 2001. Neurobiology of Pavlovian fear conditioning. Annu Rev Neurosci 24:897-931.

Maren S, Aharonov G, Fanselow MS. 1996. Retrograde abolition of conditional fear after excitotoxic lesions in the basolateral amygdala of rats: absence of a temporal gradient. Behav Neurosci 110(4):718-726.

Maren S, Quirk GJ. 2004. Neuronal signalling of fear memory. Nat Rev Neurosci 5(11):844-852.

McDonald AJ. 1987. Organization of amygdaloid projections to the mediodorsal thalamus and prefrontal cortex: a fluorescence retrograde transport study in the rat. J Comp Neurol 262(1):46-58.

Mitchell BD, Macklis JD. 2005. Large-scale maintenance of dual projections by callosal and frontal cortical projection neurons in adult mice. J Comp Neurol 482(1):17-32.

Muller JF, Mascagni F, McDonald AJ. 2006. Pyramidal cells of the rat basolateral amygdala: synaptology and innervation by parvalbumin immunoreactive interneurons. J Comp Neurol 494(4):635-650.

Ojima H. 1994. Terminal morphology and distribution of corticothalamic fibers originating from layers 5 and 6 of cat primary auditory cortex. Cereb Cortex 4(6):646-663.

Paton JJ, Belova MA, Morrison SE, Salzman CD. 2006. The primate amygdala represents the positive and negative value of visual stimuli during learning. Nature 439(7078):865-870.

Paxinos G, Huang X, Toga A. 2000. The Rhesus Monkey Brain in Stereotaxic Coordinates: ACADEMIC PRESS.

Peters A, Palay S, Webster H. 1991. The fine structure of the nervous system: neurons and their supporting cells. New York: Oxford University Press.

Phelps EA, LeDoux JE. 2005. Contributions of the amygdala to emotion processing: from animal models to human behavior. Neuron 48(2):175-187.

Pitkänen A, Amaral DG. 1993. Distribution of parvalbumin-immunoreactive cells and fibers in the monkey temporal lobe: the amygdaloid complex. J Comp Neurol 331(1):14-36.

Pitkänen A, Amaral DG. 1998. Organization of the intrinsic connections of the monkey amygdaloid complex: projections originating in the lateral nucleus. J Comp Neurol 398(3):431-458.

Porrino LJ, Crane AM, Goldman-Rakic PS. 1981. Direct and indirect pathways from the amygdala to the frontal lobe in rhesus monkeys. J Comp Neurol 198(1):121-136.

Price JL. 2003. Comparative aspects of amygdala connectivity. Ann N Y Acad Sci 985:50-58.

Price JL, Russchen FT, Amaral DG. 1987. The limbic region. II: The amygdaloid complex. In: Bjorklund AH, T. Swanson, L.W., editor. Handbook of chemical neuroanatomy. Amsterdam: Elsevier Science. p 279-388.

Ray JP, Price JL. 1993. The organization of projections from the mediodorsal nucleus of the thalamus to orbital and medial prefrontal cortex in macaque monkeys. J Comp Neurol 337(1):1-31.

Rockland KS. 1996. Two types of corticopulvinar terminations: round (type 2) and elongate (type 1). J Comp Neurol 368(1):57-87.

Rockland KS. 1998. Convergence and branching patterns of round, type 2 corticopulvinar axons. J Comp Neurol 390(4):515-536.

Rouiller EM, Welker E. 2000. A comparative analysis of the morphology of corticothalamic projections in mammals. Brain Res Bull 53(6):727-741.

Russchen FT, Amaral DG, Price JL. 1987. The afferent input to the magnocellular division of the mediodorsal thalamic nucleus in the monkey, Macaca fascicularis. J Comp Neurol 256(2):175-210.

Russchen FT, Bakst I, Amaral DG, Price JL. 1985. The amygdalostriatal projections in the monkey. An anterograde tracing study. Brain Res 329(1-2):241-257.

Saddoris MP, Gallagher M, Schoenbaum G. 2005. Rapid associative encoding in basolateral amygdala depends on connections with orbitofrontal cortex. Neuron 46(2):321-331.

Schoenbaum G, Setlow B, Saddoris MP, Gallagher M. 2003. Encoding predicted outcome and acquired value in orbitofrontal cortex during cue sampling depends upon input from basolateral amygdala. Neuron 39(5):855-867.

Schwartz ML, Dekker JJ, Goldman-Rakic PS. 1991. Dual mode of corticothalamic synaptic termination in the mediodorsal nucleus of the rhesus monkey. J Comp Neurol 309(3):289-304.

Sensi SL, Jeng JM. 2004. Rethinking the excitotoxic ionic milieu: the emerging role of Zn(2+) in ischemic neuronal injury. Curr Mol Med 4(2):87-111.

Sherman SM, Guillery RW. 1998. On the actions that one nerve cell can have on another: distinguishing "drivers" from "modulators". Proc Natl Acad Sci U S A 95(12):7121-7126.

Sherman SM, Guillery RW. 2001. Exploring the thalamus. San Diego: Academic Press.

Slomianka L. 1992. Neurons of origin of zinc-containing pathways and the distribution of zinc-containing boutons in the hippocampal region of the rat. Neuroscience 48(2):325-352.

Smart TG, Hosie AM, Miller PS. 2004. Zn2+ ions: modulators of excitatory and inhibitory synaptic activity. Neuroscientist 10(5):432-442.

Sugase-Miyamoto Y, Richmond BJ. 2005. Neuronal signals in the monkey basolateral amygdala during reward schedules. J Neurosci 25(48):11071-11083.

Swanson LW, Petrovich GD. 1998. What is the amygdala? Trends Neurosci 21(8):323-331.

Taktakishvili O, Sivan-Loukianova E, Kultas-Ilinsky K, Ilinsky IA. 2002. Posterior parietal cortex projections to the ventral lateral and some association thalamic nuclei in Macaca mulatta. Brain Res Bull 59(2):135-150.

Tokuno H, Hatanaka N, Chiken S, Ishizuka N. 2002. An improved method with a long-shanked glass micropipette and ultrasonography for drug injection into deep brain structure of the monkey. Brain Res Brain Res Protoc 10(1):16-22.

Tononi G, Sporns O, Edelman GM. 1992. Reentry and the problem of integrating multiple cortical areas: simulation of dynamic integration in the visual system. Cereb Cortex 2(4):310-335.

Wilensky AE, Schafe GE, Kristensen MP, LeDoux JE. 2006. Rethinking the fear circuit: the central nucleus of the amygdala is required for the acquisition, consolidation, and expression of pavlovian fear conditioning. J Neurosci 26(48):12387-12396.

Williams LM, Das P, Liddell BJ, Kemp AH, Rennie CJ, Gordon E. 2006. Mode of functional connectivity in amygdala pathways dissociates level of awareness for signals of fear. J Neurosci 26(36):9264-9271.

Zald DH. 2003. The human amygdala and the emotional evaluation of sensory stimuli. Brain Res Brain Res Rev 41(1):88-123.

Zhong YM, Rockland KS. 2003. Inferior Parietal Lobule Projections to Anterior Inferotemporal Cortex (Area TE) in Macaque Monkey. Cereb Cortex 13(5):527-540.

Zikopoulos B, Barbas H. 2006. Prefrontal projections to the thalamic reticular nucleus form a unique circuit for attentional mechanisms. J Neurosci 26(28):7348-7361.

Figure legends

Fig. 1

Coronal sections from three monkeys with BDA injections

(A) Low magnification (case 300) of an injection localized to the lateral nucleus of the amygdala.

(B) Higher magnification (case 300), of the injection site (asterisk) and intrinsic terminations (arrow), medially in the accessory basal (AB) nucleus.

(C) BDA injection (asterisk; case 298) centered in the AB nucleus. Arrowhead indicates terminations in the lateral nucleus, which may have resulted from some involvement of the overlying nucleus of Meynert.

(D) BDA injection (asterisk; case R100) located in the ventral portion of the lateral nucleus. Arrow indicates a medial patch of intrinsic terminations in the AB nucleus.

(E) Section adjacent to that in D, which has been reacted with anti-parvalbumin antibody in order to more clearly demonstrate subnuclei. The two darkened regions (in Lv and ABpc) correspond to regions of dense BDA-labeled terminations.

Scale bars = 5 mm in A, 1 mm in E (applies to B-E)

Fig. 2

Schematic view of a left cerebral hemisphere, showing the location of cortical sites with injections of anterograde tracers. Two brains (P4 and P5) had injections in parietal cortex (see also Fig. 1 of Zhong and Rockland, 2003), and three others (R42,

R43, R53) had injections within prefrontal cortex. These caseswere used t o compare the morphology of CT and AT terminations in MD.

Fig. 3

BDA-labeled AT terminations form patches in MDmc. A-H: Eight sections (299-306, 50mm thickness) through MDmc (case 298). Arrows mark the same two blood vessels in each image. Patches can occur as isolated (hollow arrowhead in D) or clustered in groups ≥ 12 (solid arrowhead in D). I: Merged image to demonstrate pattern of patches over 0.4mm thickness. Medial is a right; dorsal at top. Scale bar = 500 μm in I

Fig. 4

Individual AT arbors are small.

(A) A terminal focus made up of 12-15 delimited arbors (Higher magnification from solid arrowhead in Fig. 2D).

(B and C) Higher magnification of two arbors. Note spoke-like configuration and close association with cell bodies (at three arrows). The close association is suggestive of a proximal postsynaptic location.

(D) Higher magnification of one arbor from arrowhead in A. Spoke-like configurations are located close to the cell body (arrow).

Scale bar = 100 μm in A, 10 μm in D (applies to B-D)

Fig. 5

AT arbors appear to target proximal portions.

(A) AT terminations (case 298) are shown with cell bodies (unlabeled) in MDmc.

(B and C) For comparison, type-2 cortico-thalamic terminations, in MDmc, labeled by a BDA injection in the inferior parietal cortex. These are closely associated with retrogradely labeled thalamo-cortical neurons in MD.

Scale bars = 50 μm in A, 20 μm in C (applies to B and C)

Fig. 6

Camera lucida reconstruction through 8 sections (306-313; 400 μm) of BDA-labeled AT terminations in MDmc. One axon (black solid arrowhead, pointing away from distal portion) has three arbors, two of which converge from a proximal bifurcation. A second axon (red hollow arrowhead, pointing away from the distal portion) has one arbor, which overlaps with the convergent focus. Dotted circles schematically represent terminal arbors (See also Fig. 7A). Medial is at right; dorsal at top. Scale bar = 200 μm

Fig. 7

(A) Photomicrograph of the converging arbors of the axon shown in Fig. 6. Arrowhead indicates red axon in Fig. 6. (B) Another example of convergence and divergence. In this section, one axon (arrowheads) can be seen to have two converging branches (hollow arrowhead), to a more distal terminate focus. Scale bars = 100 μm

Fig. 8

AT boutons are large, but with some variability

(A) AT terminations in MDmc from the accessory basal nucleus (case 298).

(B) Higher-magnification, from arrow in A, to show large oval boutons surrounded by threadlike processes.

(C) Higher magnification from arrowhead in A, to show a distal group of four boutons, including a relatively long, filopodia-like structure.

(D and E) Mixed large and small boutons occur together in close proximity along the same arbor. These segments also illustrate typical rows or cartridges, consisting of 5-7 rather uniform, closely packed beaded boutons (arrowheads) .

Scale bars = 50 μm in A, 10 μm in E (applies to B and E)

Fig. 9

Distinctive phenotypes of terminations from different projection systems.

(A) Small-bouton AC terminations in layer 2 of prefrontal area 12.

(B) Large-bouton AT terminations in MDmc (case R100).

(C) Small-bouton, spinous ("drumstick") CT terminations in MD (from prefrontal area 12).

(D) Large-bouton cortico-pulvinar terminations (from inferior parietal lobule).

Scale bar = 10 μm in D

Fig. 10

Cortical areas, but not thalamic nuclei, are rich in synaptic Zn.

(A) Coronal section of PFC, where the orbitofrontal cortex is especially Zn-rich (arrow).

(B) Coronal section at the level of the mid -LGN, to demonstrate the extremely low level of synaptic Zn in the thalamus (star).

(C) Section adjacent to B, stained for PV, to show thalamic nuclear subdivisions.

Scale bar = 5 mm in C

Fig. 11

The laminar distribution of Zn+ terminations coincides with that of AC terminations.

(A) Coronal section of the orbitfrontal cortex, where Zn+ terminations are densest in layers 1b, 2, 5 and upper 6.

(B) Adjacent section with BDA-labeled amygdalo-cortical terminations. These are densest in layer2 and upper 3.

Scale bar = 200 μm in B

Fig. 12

Electron micrographs of six AC terminations that are labeled by BDA and are also Zn+. (A) Termination onto spine (s), in the supragranular layers of medial prefrontal cortex (area 25, case 298). Solid black spots correspond to silver intensification of zinc selenite crystals.

(B) Zn+ BDA-labeled AC synapse, from the same region as in A, contacting a dendritic shaft (d).

(C) Zn+ BDA-labeled synapse, from the deeper layers of the same region, contacting a dendritic spine (s, case 298).

(D) Zn+ BDA-labeled synapse, from the infragranular layers of area 25 (case 100), contacting a dendritic spine (s).

(E and F) Fenestrated terminations onto a spine (s, E) and a dendritic shaft (d, F) (case R100). Arrowheads point to postsynaptic thickenings.

Scale bar = 0.5 μm in A

Fig. 13

Diagram summarizing the characteristics of AT and AC terminations. AT terminations are typically large, and form small arbors. AC terminations are small, and form widespread arbors. The projections appear to originate from two populations of neurons in the amygdala. AC terminations, but not AT, are Zn-positive.

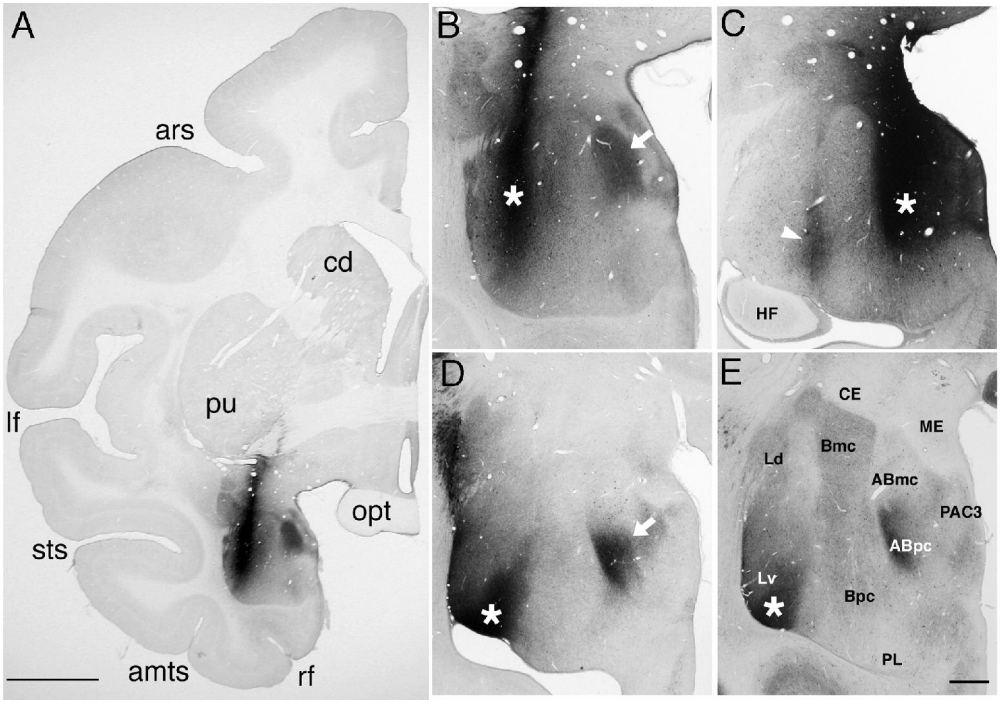

Fig. 1 Coronal sections from three monkeys with BDA injections (A) Low magnification (case 300) of an injection localized to the lateral nucleus of the amygdala. (B) Higher magnification (case 300), of the injection site (asterisk) and intrinsic terminations (arrow), medially in the accessory basal (AB) nucleus. (C) BDA injection (asterisk; case 298) centered in the AB nucleus. Arrowhead indicates terminations in the lateral nucleus, which may have resulted from some involvement of the overlying nucleus of Meynert. (D) BDA injection (asterisk; case R100) located in the ventral portion of the lateral nucleus. Arrow indicates a medial patch of intrinsic terminations in the AB nucleus. (E) Section adjacent to that in D, which has been reacted with anti-parvalbumin antibody in order to more clearly demonstrate subnuclei. The two darkened regions (in Lv and ABpc) correspond to regions of dense BDA-labeled terminations. Scale bars = 5 mm in A, 1 mm in E (applies to B-E)

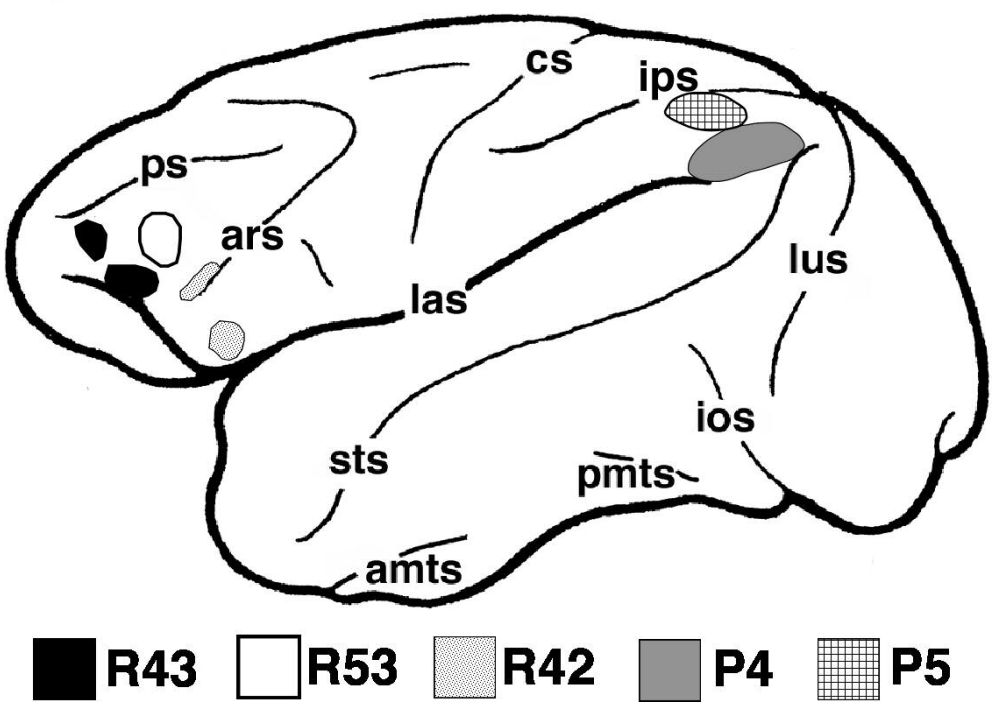

Fig. 2 Schematic view of a left cerebral hemisphere, showing the location of cortical sites with injections of anterograde tracers. Two brains (P4 and P5) had injections in parietal cortex (see also Fig. 1 of Zhong and Rockland, 2003), and three others (R42, R43, R53) had injections within prefrontal cortex. These cases were used to compare the morphology of CT and AT terminations in MD.

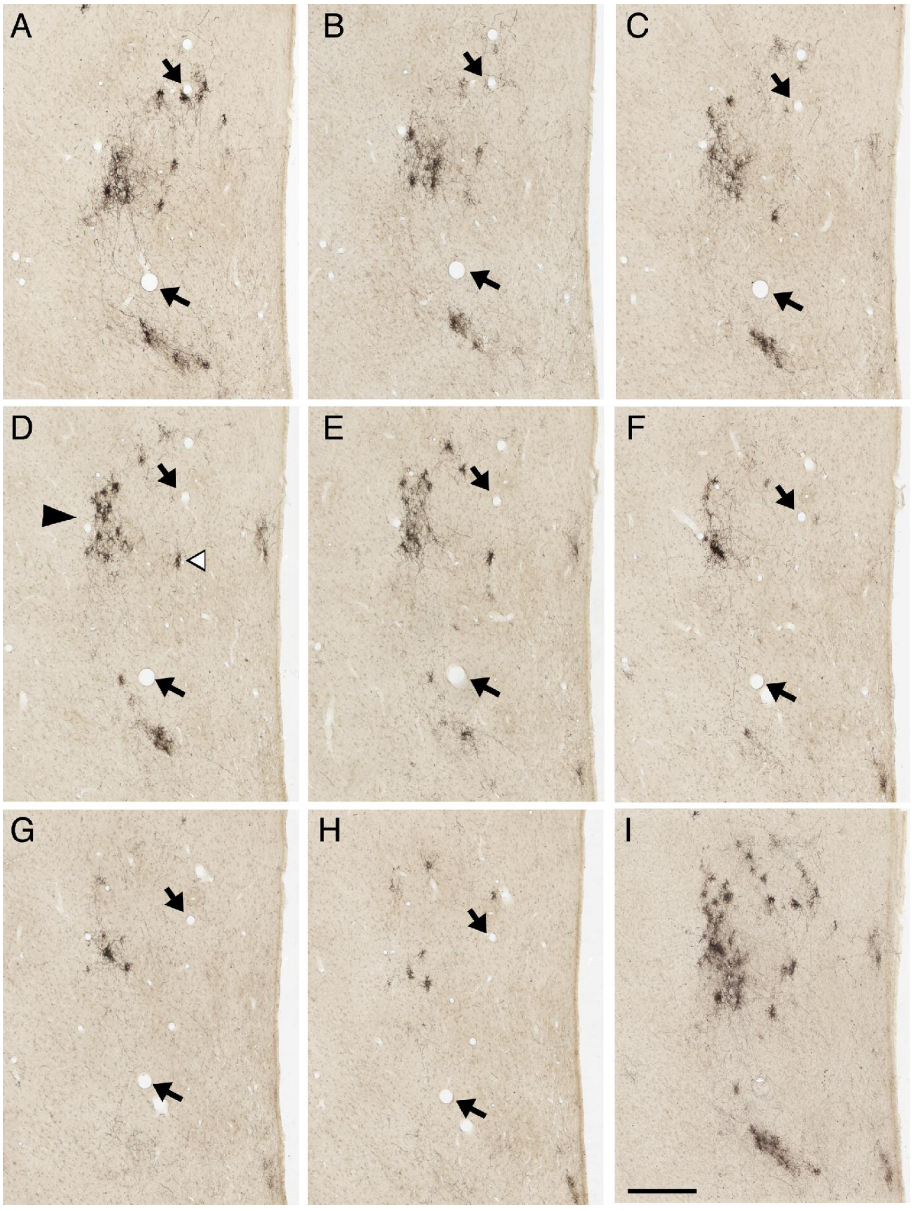

Fig. 3 BDA-labeled AT terminations form patches in MDmc. A-H: Eight sections (299-306, 50mm thickness) through MDmc (case 298). Arrows mark the same two blood vessels in each image. Patches can occur as isolated (hollow arrowhead in D) or clustered in groups ≥12 (solid arrowhead in D). I: Merged image to demonstrate pattern of patches over 0.4mm thickness. Medial is a right; dorsal at top. Scale bar = 500 μm in I

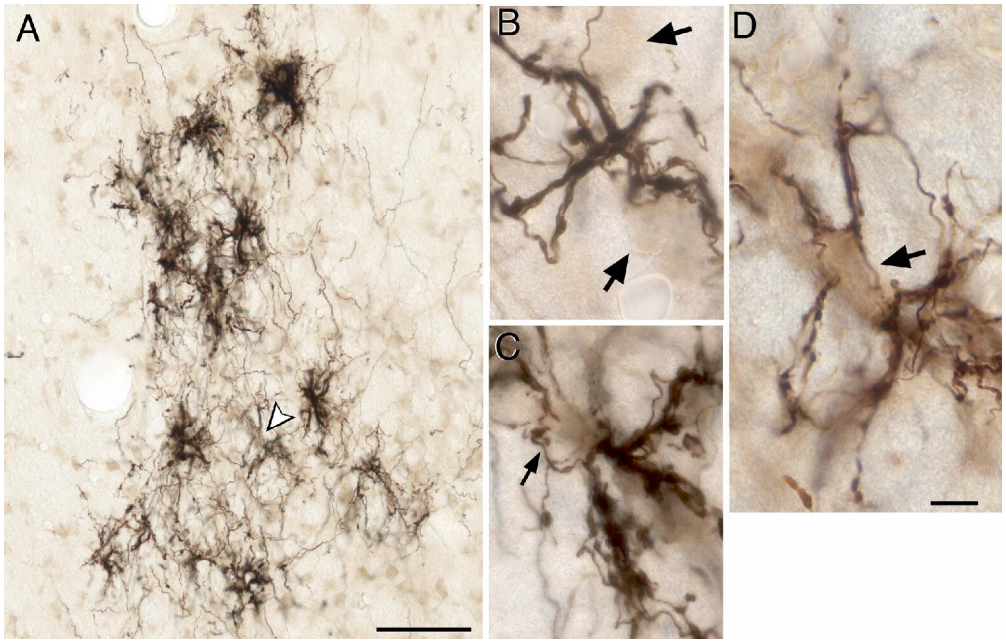

Fig. 4 Individual AT arbors are small. (A) A terminal focus made up of 12-15 delimited arbors (Higher magnification from solid arrowhead in Fig. 2D). (B and C) Higher magnification of two arbors. Note spoke-like configuration and close association with cell bodies (at three arrows). The close association is suggestive of a proximal postsynaptic location. (D) Higher magnification of one arbor from arrowhead in A. Spoke-like configurations are located close to the cell body (arrow). Scale bar = 100 μm in A, 10 μm in D (applies to B-D)

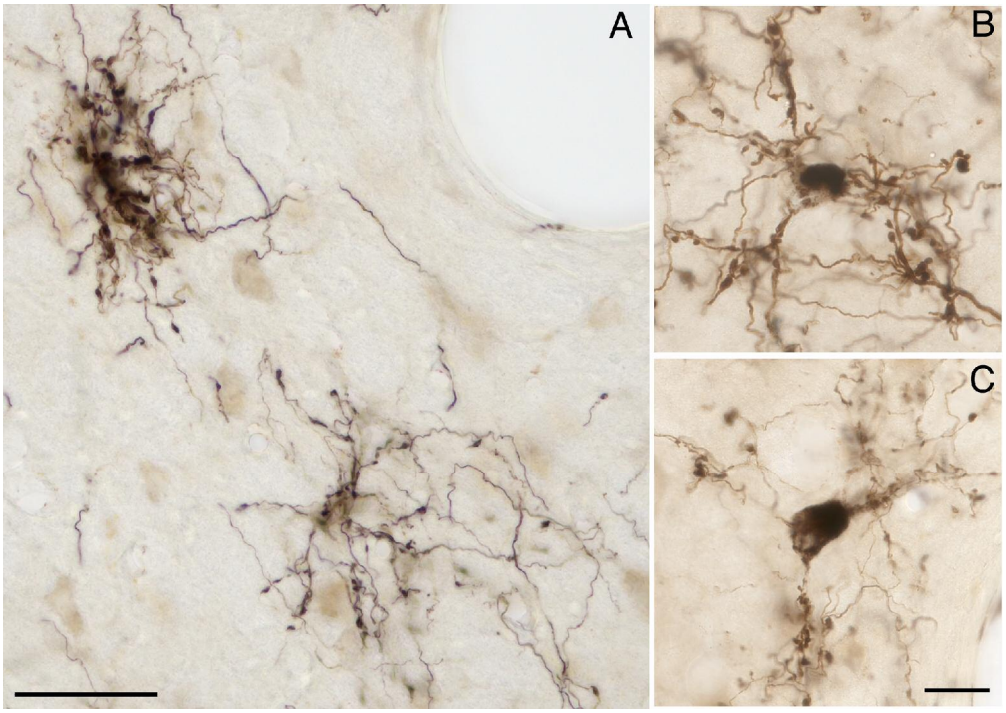

Fig. 5 AT arbors appear to target proximal portions. (A) AT terminations (case 298) are shown with cell bodies (unlabeled) in MDmc. (B and C) For comparison, type-2 cortico-thalamic terminations, in MDmc, labeled by a BDA injection in the inferior parietal cortex. These are closely associated with retrogradely labeled thalamo-cortical neurons in MD. Scale bars = 50 μm in A, 20 μm in C (applies to B and C)

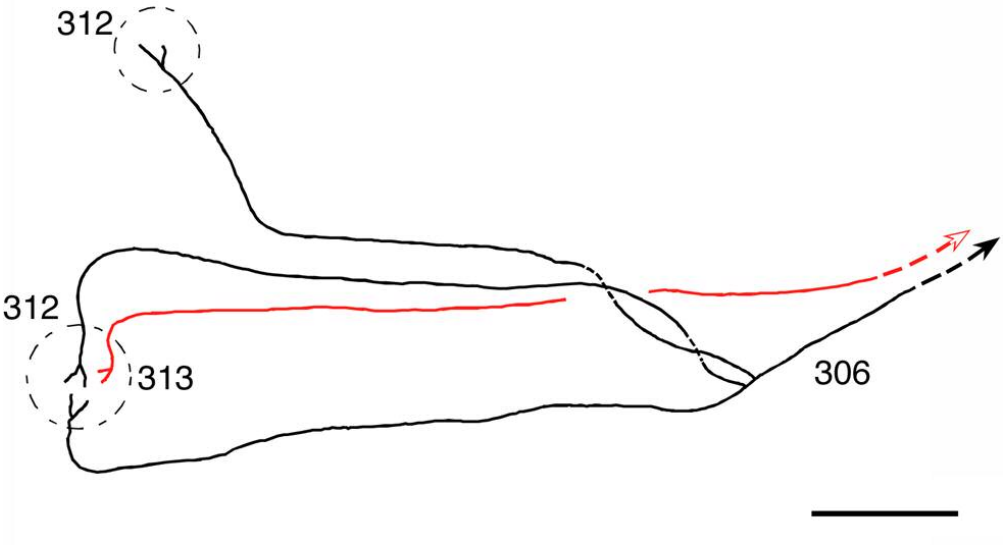

Fig. 6 Camera lucida reconstruction through 8 sections (306-313; 400 μm) of BDA-labeled AT terminations in MDmc. One axon (black solid arrowhead, pointing away from distal portion) has three arbors, two of which converge from a proximal bifurcation. A second axon (red hollow arrowhead, pointing away from the distal portion) has one arbor, which overlaps with the convergent focus. Dotted circles schematically represent terminal arbors (See also Fig. 7A). Medial is at right; dorsal at top. Scale bar = 200 μm

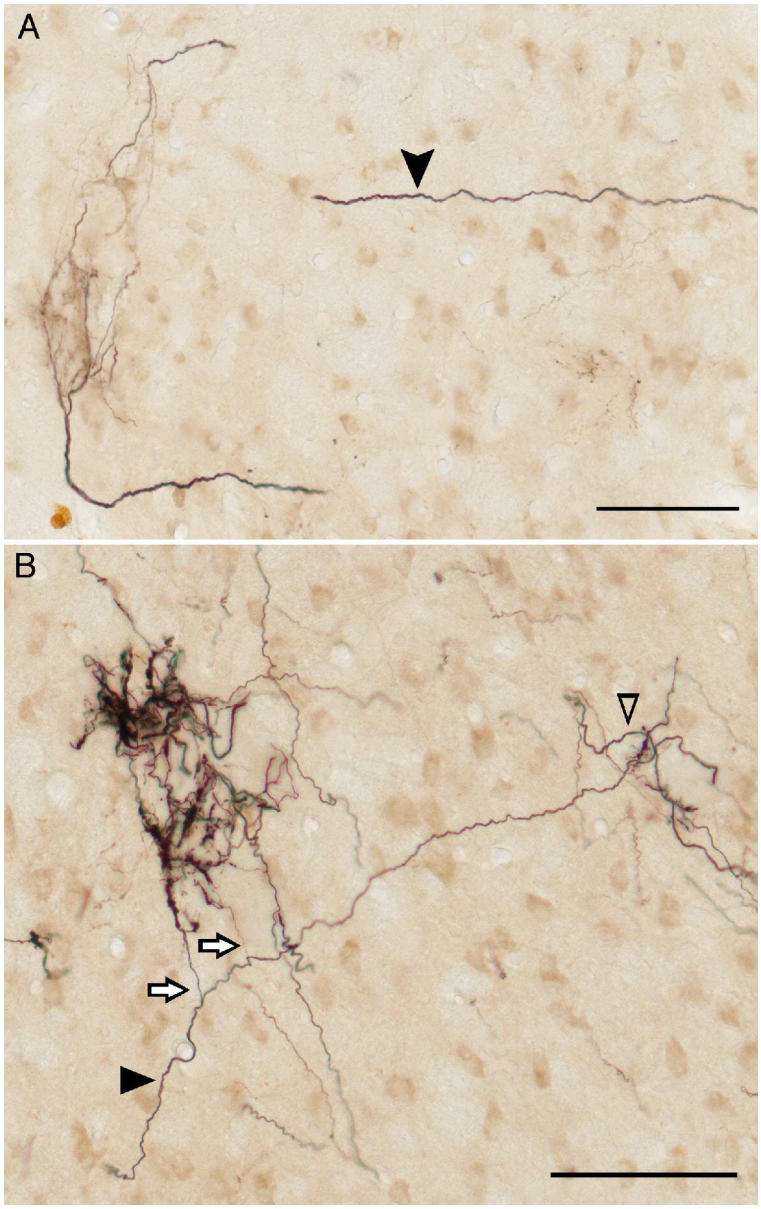

Fig. 7 (A) Photomicrograph of the converging arbors of the axon shown in Fig. 6. Arrowhead indicates red axon in Fig. 6. (B) Another example of convergence and divergence. In this section, one axon (arrowheads) can be seen to have two converging branches (hollow arrowhead), to a more distal terminate focus. Scale bars = 100 μm

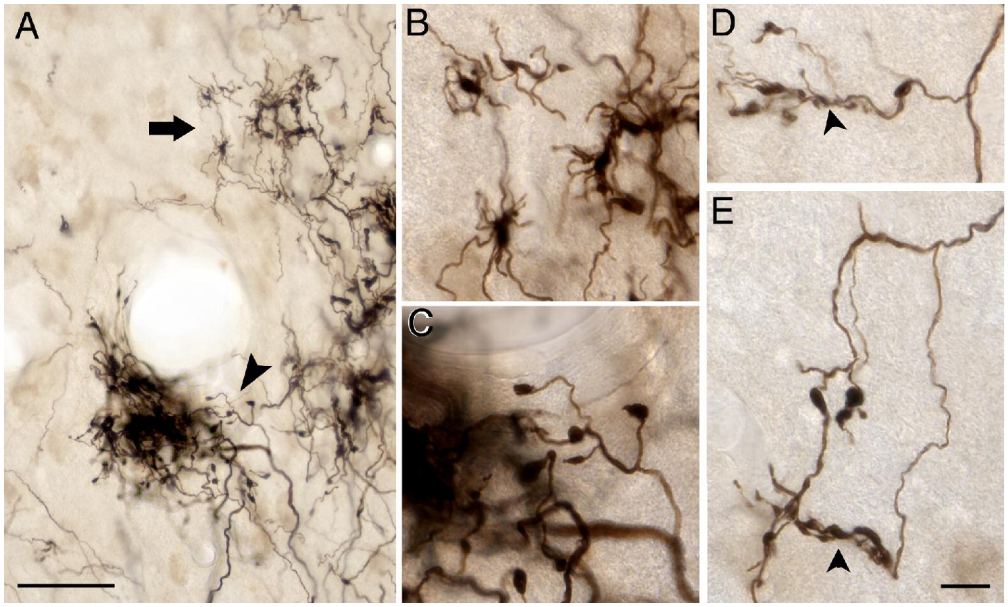

Fig. 8 AT boutons are large, but with some variability (A) AT terminations in MDmc from the accessory basal nucleus (case 298). (B) Higher-magnification, from arrow in A, to show large oval boutons surrounded by threadlike processes. (C) Higher magnification from arrowhead in A, to show a distal group of four boutons, including a relatively long, filopodia-like structure. (D and E) Mixed large and small boutons occur together in close proximity along the same arbor. These segments also illustrate typical rows or cartridges, consisting of 5-7 rather uniform, closely packed beaded boutons (arrowheads) . Scale bars = 50 μm in A, 10 μm in E (applies to B and E)

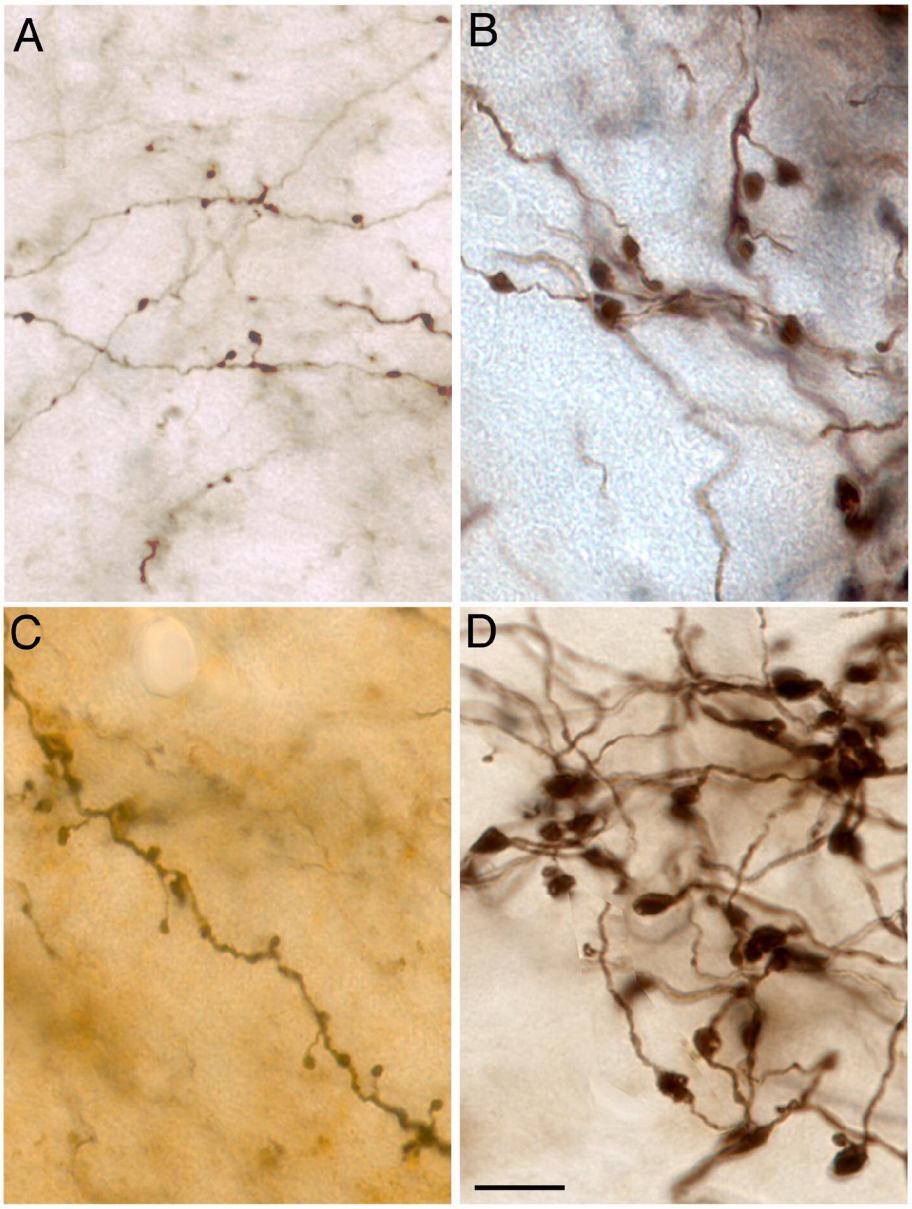

Fig. 9 Distinctive phenotypes of terminations from different projection systems. (A) Small-bouton AC terminations in layer 2 of prefrontal area 12. (B) Large-bouton AT terminations in MDmc (case R100). (C) Small-bouton, spinous (□gdrumstick□h) CT terminations in MD (from prefrontal area 12). (D) Large-bouton cortico-pulvinar terminations (from inferior parietal lobule). Scale bar = 10 μm in D

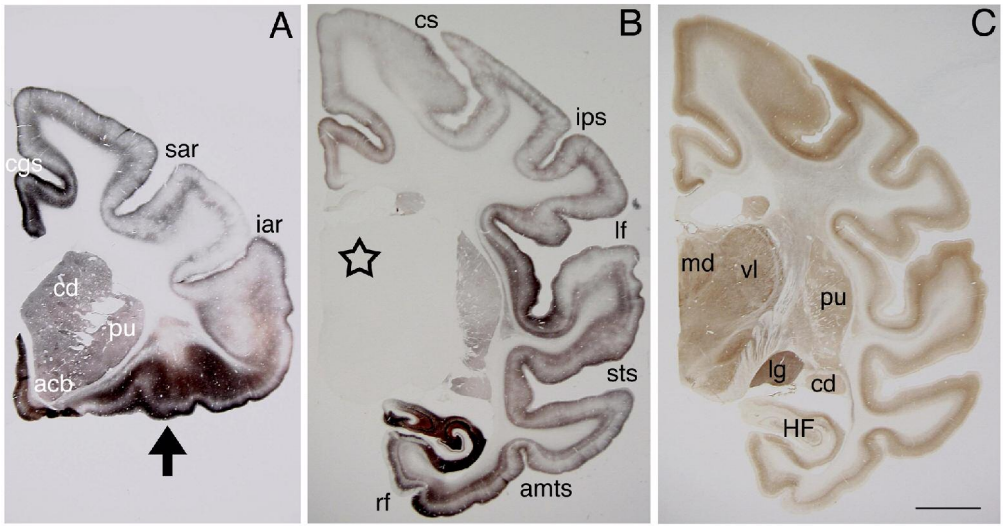

Fig. 10 Cortical areas, but not thalamic nuclei, are rich in synaptic Zn. (A) Coronal section of PFC, where the orbitofrontal cortex is especially Zn-rich (arrow). (B) Coronal section at the level of the mid -LGN, to demonstrate the extremely low level of synaptic Zn in the thalamus (star). (C) Section adjacent to B, stained for PV, to show thalamic nuclear subdivisions. Scale bar = 5 mm in C

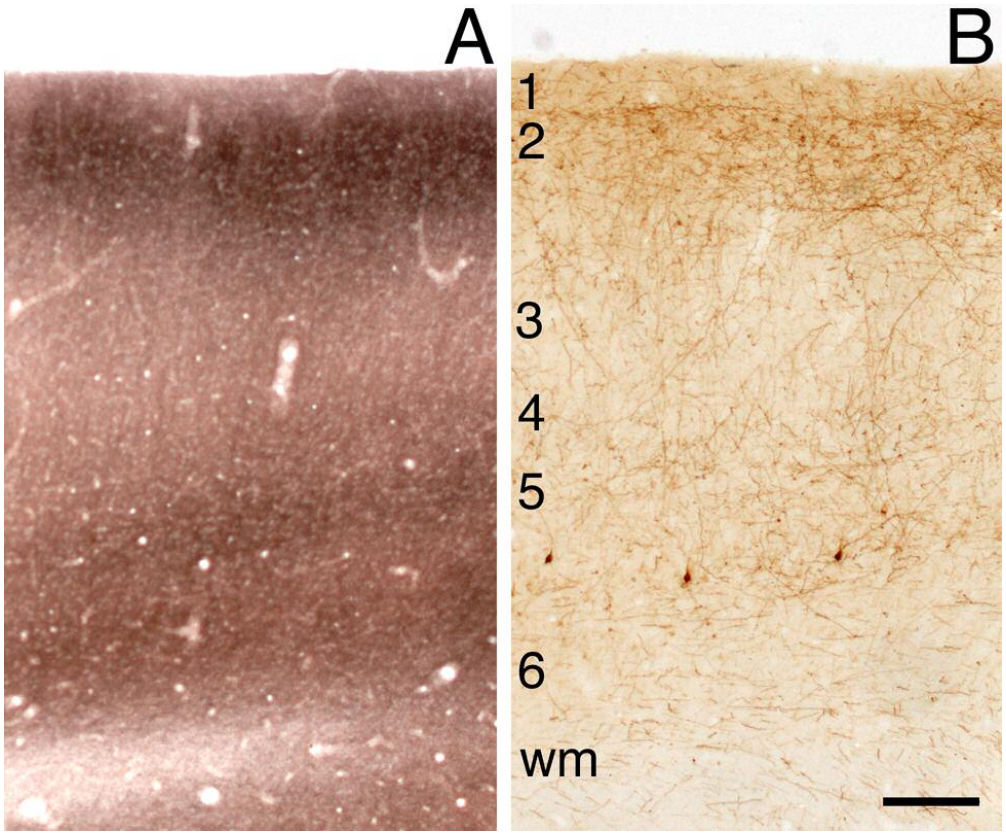

Fig. 11 The laminar distribution of Zn+ terminations coincides with that of AC terminations. (A) Coronal section of the orbitfrontal cortex, where Zn+ terminations are densest in layers 1b, 2, 5 and upper 6. (B) Adjacent section with BDA-labeled amygdalo-cortical terminations. These are densest in layer2 and upper 3. Scale bar = 200 μm in B

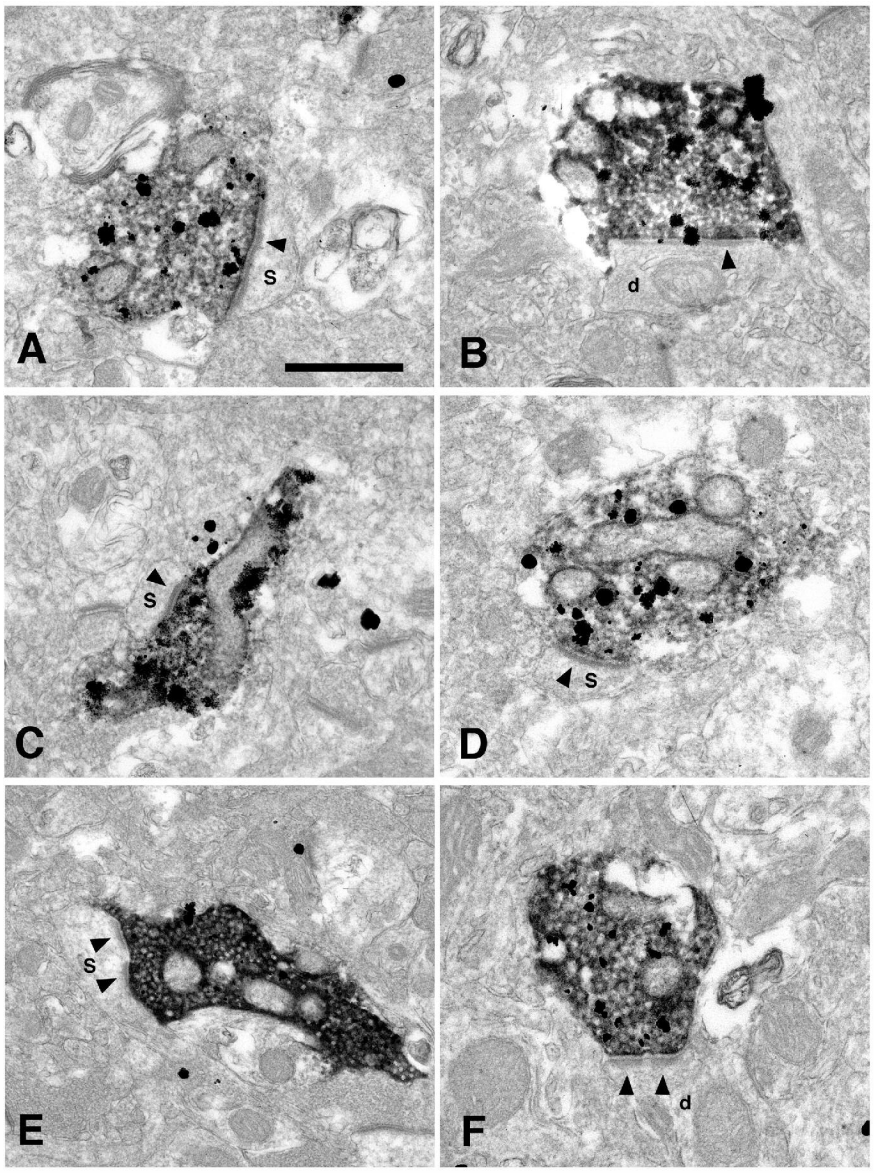

Fig. 12 Electron micrographs of six AC terminations that are labeled by BDA and are also Zn+. (A) Termination onto spine (s), in the supragranular layers of medial prefrontal cortex (area 25, case 298). Solid black spots correspond to silver intensification of zinc selenite crystals. (B) Zn+ BDA-labeled AC synapse, from the same region as in A, contacting a dendritic shaft (d). (C) Zn+ BDA-labeled synapse, from the deeper layers of the same region, contacting a dendritic spine (s, case 298). (D) Zn+ BDA-labeled synapse, from the infragranular layers of area 25 (case 100), contacting a dendritic spine (s). (E and F) Fenestrated terminations onto a spine (s, E) and a dendritic shaft (d, F) (case R100). Arrowheads point to postsynaptic thickenings. Scale bar = 0.5 μm in A

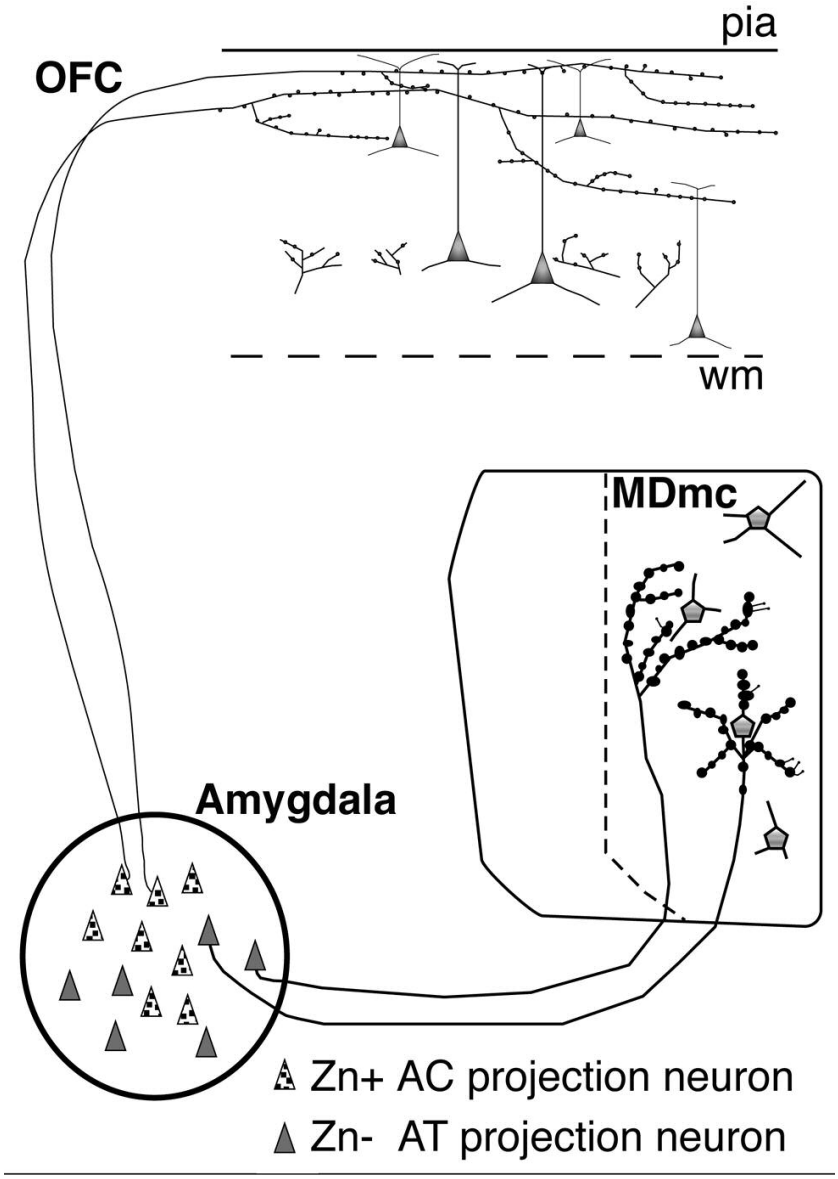

Fig. 13 Diagram summarizing the characteristics of AT and AC terminations. AT terminations are typically large, and form small arbors. AC terminations are small, and form widespread arbors. The projections appear to originate from two populations of neurons in the amygdala. AC terminations, but not AT, are Zn-positive.

Table 1. Summary of amygdaloid injection

Case	BDA injection	Injection approach	Survival (days)	Body weight (kg)
298	AB	Vertical	20	3.8
300	Ldi	Vertical	16	4.4
R100	Lv	Oblique	16	5.5

Table 2. Size of AT terminals in MDmc (in μm)

Case	Number	Median	Maximum	Minimum	Average
298	60	3.68	6.44	1.19	3.67
300	60	3.68	7.36	1.38	3.63
R100	60	2.89	6.44	1.38	3.17